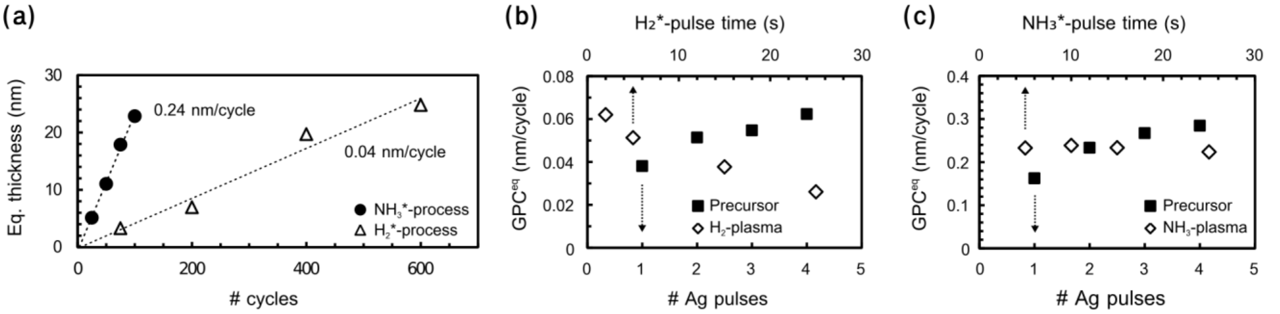

**Fig. 1**. Due to the high roughness of the ALD Ag-films, it was not possible to determine their thickness using x-ray reflectivity (XRR). Instead, we determined an equivalent thickness using x-ray fluorescence, by calibrating the integrated Ag L peak intensity with the XRR-thickness of sputtered Ag-films. GPC$^{eq}$ is defined as the increase of equivalent Ag film thickness per ALD cycle. **(a):** Equivalent Ag film thickness as a function of the number of cycles for the H$_2$* and NH$_3$*-processes on sputtered Au substrates. **(b)** and **(c):** Saturation of GPC$^{eq}$ with the precursor and plasma pulse times for the H$_2$*-process and the NH$_3$*-process, respectively. Again, sputtered Au substrates were used to avoid nucleation effects.

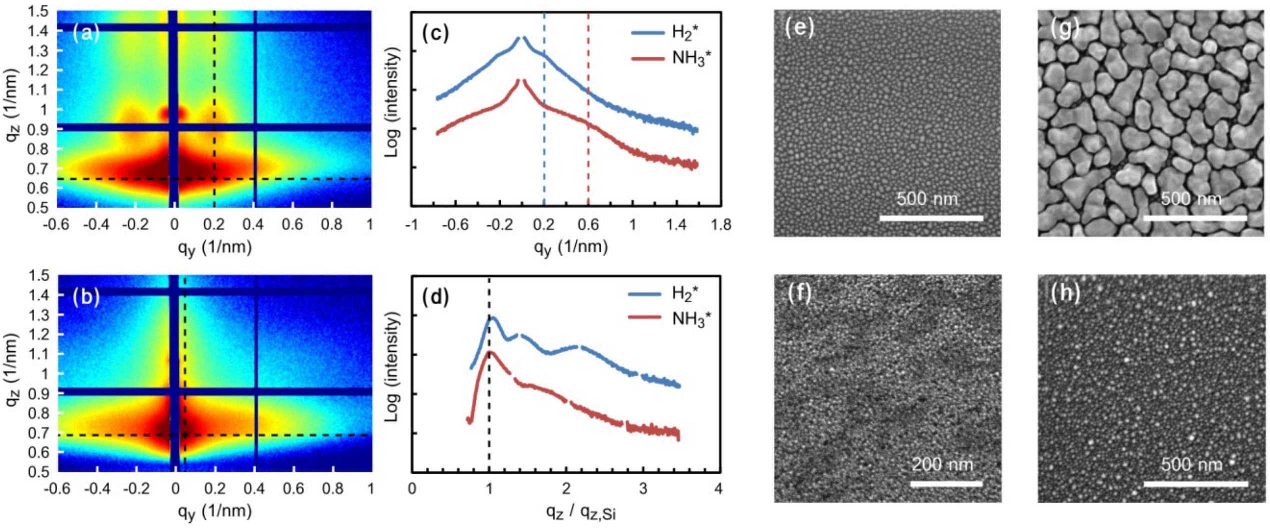

**Fig. 2**. **(a):** GISAXS pattern for a Ag film grown with 75 cycles of the H$_2$*-process on SiO$_2$. **(b):** GISAXS pattern for a Ag film grown with 20 cycles of the NH$_3$*-process on SiO$_2$. **(c):** Horizontal cuts, indicated by the horizontal black dotted lines in (a) and (b). The positions of the local maxima are indicated by the red and blue dotted lines, and these are inversely related to the center-to-center particle distance D. Estimating the particle areal density as 1/D$^2$, we find that it is 9 times larger for the NH$_3$*-process compared to the H$_2$*-process. **(d):** Vertical cuts, indicated by the vertical black dotted lines in (a) and (b). The first maxima are observed at the Si Yoneda position ($q_z/q_{z,Si} = 1$), which means that the films are discontinuous. **(e):** SEM micrograph of the sample in (a). **(f):** SEM micrograph of the sample in (b). **(g):** SEM micrograph of a Ag film grown with 400 cycles of the H$_2$*-process on SiO$_2$ **(h):** SEM micrograph of a Ag film grown with 100 cycles of the NH$_3$*-process on SiO$_2$. The films in (e) and (f) were selected for their comparable equivalent thickness of ~ 5nm, and for (g) and (h) this was ~ 40 nm.

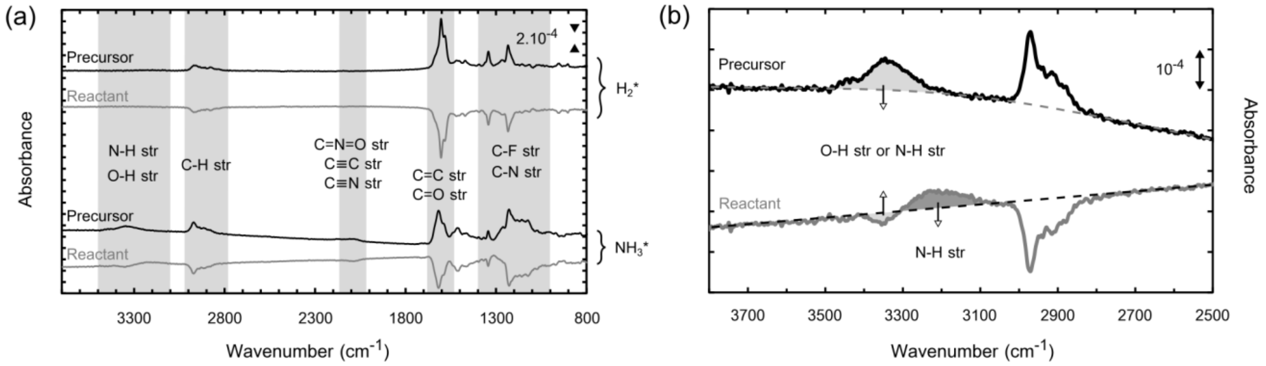

**Fig. 3. (a):** Steady state FTIR difference spectra of both half cycles for the H$_2$* and NH$_3$*-process on SiO$_2$. The expected peak positions of several molecular vibrations are given by the vertical grey bands. There are three features which are only present for the NH$_3$*-process: there is a broad band in the region 3100-3500 cm$^{-1}$, a weak peak around ~2100 cm$^{-1}$, and a broad feature at 1100-1200 cm$^{-1}$. As can be seen, each of these features can be possibly related to N-containing surface groups. **(b):** A zoom of the FTIR data for the NH$_3$*-process in the region of the N-H, O-H and C-H stretches. The dotted lines are suggestions for the background. As the dark shaded absorbance peak doesn't have a negative counterpart in the precursor difference spectrum, this suggests that these surface groups are being built into the growing film. If we attribute this peak to N-H stretching vibrations, this could explain the observed N-impurities by XPS. The light shaded absorbance peak in the precursor difference spectrum does have a negative counterpart. As the precursor contains oxygen atoms, it is plausible that O-H stretching vibrations are responsible for this peak. However, this peak was not present for the H$_2$*-process. It is also possible that this peak arises through N-H stretching vibrations, for example due to amines formed by interaction of the surface groups present after the NH$_3$*-pulse with the incoming precursor. These can have a shifted wavelength of the N-H stretching vibration relative to the dark shaded peak due to a different bonding. If we return to (a), the other peaks that were only present for the NH$_3$*-process (at ~2100 cm$^{-1}$ and 1100-1200 cm$^{-1}$) and are possibly related to N-containing surface groups, are positive in the precursor difference spectrum. Again, these surface groups can be created through an interaction of the N-containing surface groups present after the NH$_3$*-pulse with the incoming precursor molecules, which could result in a more efficient removal of precursor-ligands compared to the H$_2$*-process.